

---

# SOLAR WIND CURRENT SHEETS: MVA INACCURACY AND RECOMMENDED SINGLE-SPACECRAFT METHODOLOGY

---

A PREPRINT

**Rachel Wang\***

Space Sciences Laboratory, University of California at Berkeley, California, CA94720, USA  
rw6831@princeton.edu

Ivan Y. Vasko

Space Sciences Laboratory, University of California at Berkeley, California, CA94720, USA  
Space Research Institute of Russian Academy of Sciences, Moscow, 117997, Russia

Tai Phan

Space Sciences Laboratory, University of California at Berkeley, California, CA94720, USA

Forrest S. Mozer

Space Sciences Laboratory, University of California at Berkeley, California, CA94720, USA

December 12, 2023

## ABSTRACT

We present the analysis of 2,033 current sheets (CS) observed aboard four Cluster spacecraft in a pristine solar wind. Four-spacecraft estimates of the CS normal and propagation velocity are compared with different single-spacecraft estimates. The Minimum Variance Analysis (MVA) of the magnetic field is shown to be highly inaccurate in estimating the normal. The MVA normal often differs by more than  $60^\circ$  from the normal obtained by multi-spacecraft timing method, likely due to ambient turbulent fluctuations. In contrast, the cross-product of magnetic fields at the CS boundaries delivers the normal with the uncertainty of less than  $15^\circ$  at the confidence level of 90%. The CSs are essentially frozen into plasma flow, since their propagation velocity is consistent with local ion flow velocity within 20% at the confidence level of 90%. The single-spacecraft methodology based on the cross-product method and frozen-in assumption delivers the CS thickness and current density amplitude within 20% of their actual values at the confidence level of 90%. The CSs are kinetic-scale structures with half-thickness  $\lambda$  from a few tenths to tens of local proton inertial length  $\lambda_p$  and scale-dependent shear angle and current density amplitude,  $\Delta\theta \propto (\lambda/\lambda_p)^{0.5}$  and  $J_0 \propto (\lambda/\lambda_p)^{-0.5}$ . The classification of the CSs in terms of tangential and rotational discontinuities remains a challenge, because even the four-spacecraft normal has too large uncertainties to reveal the actual normal magnetic field component. The presented results will be valuable for the analysis of solar wind CSs, when only single-spacecraft measurements are available.

**Keywords** solar wind, · turbulence · current sheets

## 1 Introduction

The early spacecraft measurements revealed the presence of directional discontinuities or, equivalently, current sheets in the solar wind at various radial distances from the Sun [1, 2, 3, 4, 5, 6, 7]. The modern spacecraft measurements with higher temporal resolution demonstrated that solar wind current sheets are much more abundant than previously

---

\*currently at Princeton University, New Jersey, USA

thought and have spatial thickness from a fraction to a few tens of proton inertial lengths [8, 9, 10, 11, 12, 13, 14]. It has been demonstrated that current sheets are substantially contributing into turbulence spectrum [15, 16] and correlated with enhanced electron and ion temperatures in the solar wind [17, 18, 19, 20]. Even though a fraction of the strongest current sheets can potentially originate in solar corona [21, 22], there is a strong evidence that the majority of solar wind current sheets are produced locally by turbulence cascade [8, 23, 24, 25, 13, 14]. Similar coherent structures are indeed naturally formed in numerical simulations of plasma turbulence and substantially contribute into turbulence dissipation even though they occupy a relatively small volume [26, 27, 28, 29, 30, 31, 32]. Among the processes leading to turbulence dissipation is magnetic reconnection that has been observed in the solar wind [33, 34, 35, 36, 37, 38, 39, 40] as well as turbulence simulations [41, 42, 43, 44, 45]. The analysis of solar wind current sheets is therefore valuable not only for modelling solar wind turbulence, but also for understanding magnetic reconnection and plasma heating in turbulence in general.

Spacecraft measurements showed that the magnetic field across solar wind current sheets typically rotates through some shear angle, but does not essentially vary in magnitude [1, 2, 3, 4, 8, 11, 12]. The early studies were mostly based on single-spacecraft measurements, where current sheets were assumed locally planar one-dimensional structures frozen into the plasma flow (Taylor hypothesis), while current sheet normals were computed using Minimum Variance Analysis [2, 3, 46, 5, 6, 7]. These studies were heavily focused on classifying solar wind current sheets in terms of tangential or rotational discontinuities based on the magnitude of the normal magnetic field component. Multi-spacecraft observations demonstrated however that Minimum Variance Analysis provides *highly inaccurate* estimates of current sheet normals in the solar wind and questioned thereby validity of these classifications [47, 48]. Four-spacecraft Cluster measurements allowed estimating the normal by the timing method and showed that the normal magnetic field component is typically much smaller than local magnetic field magnitude and often within methodology uncertainties [48]. Thus, solar wind current sheets can be tangential discontinuities and/or rotational discontinuities with a small normal component. The relative occurrence of the different discontinuities in the solar wind is still not known [49, 50, 51, 52].

Knetter et al., 2004 [48] showed that the most accurate single-spacecraft estimate of the current sheet normal is delivered by the cross-product of magnetic fields at the current sheet boundaries. The recent statistical studies of various properties of solar wind current sheets at 0.2 and 1 AU have been based on a single-spacecraft methodology relying on the cross-product normals [8, 12, 13, 14] and similar methodology has been widely used in the analysis of magnetic reconnection [53, 38, 39, 35, 40]. This single-spacecraft methodology needs to be thoroughly tested however, since even though Knetter et al., 2004 [48] demonstrated the reliability of the cross-product normals, their analysis was limited to only about a hundred current sheets. Even more critical is that the selection procedure used by Knetter et al., 2004 [48] was biased toward current sheets, whose thickness and shear angle were respectively larger than about 1,000 km and  $30^\circ$ . The occurrence rate of these current sheets turned out to be less than one per hour. The recent studies showed however that solar wind current sheets at 1 AU are actually at least one order of magnitude more abundant and the most of current sheets have much smaller thickness and shear angle [8, 10, 12, 13].

In this paper we present the analysis of more than two thousand current sheets observed aboard four Cluster spacecraft in a pristine solar wind. We substantially expand the previous multi-spacecraft studies by collecting a factor of ten more current sheets. Importantly, the collected dataset is not merely larger, but, in contrast to previous studies, also representative of solar wind current sheets typically present at 1 AU. Using this extensive and representative dataset we quantify the accuracy of the estimates of current sheet properties by the single-spacecraft methodology based on the cross-product normal and frozen-in assumption (Taylor hypothesis). Using the collected extensive dataset we show that Minimum Variance Analysis (MVA) is indeed highly inaccurate in estimating current sheet normals independent of the theoretical indicator of MVA accuracy, the ratio between intermediate and minimum eigenvalues. We demonstrate that the single-spacecraft methodology used in the recent statistical studies delivers relatively accurate estimates of the current sheet properties including thickness and current density magnitude. The latter result is of value for modern studies of the solar wind near the Sun and beyond 1 AU, where only single-spacecraft measurements are available. Based on estimates of current sheet properties we discuss the nature and origin of current sheets in the solar wind.

## 2 Data and methodology

## 3 Data and methodology

We used the following data provided by Cluster spacecraft [54, 55]: magnetic field measurements at blue22 S/s (Samples per second) resolution provided by Flux Gate Magnetometer [56], ion flow velocity at 4s cadence provided by CIS/HIA (Cluster Ion Spectrometry/Hot Ion Analyzer) instrument [57], electric field spectra from about 2 to 80 kHz at 0.1s cadence and electron density estimates at 2s cadence provided by the Whisper instrument [58]. Note that we used proton flow velocity at 8s cadence provided by CIS/CODIF (Composition and Distribution Function) instrument [57] for the interval presented in Figure 1, because CIS/HIA moments were not available. We visually inspected proton

and electron pitch-angle distributions provided at a few second cadence respectively by CIS/CODIF [57] and Plasma Electron and Current Experiment [59]. We also used proton temperature estimates provided by Wind spacecraft [60]. Note that plasma density estimates provided by the Whisper instrument aboard Cluster were consistent within 25% with plasma density estimates provided by Wind spacecraft. Below the Geocentric Solar Ecliptic (GSE) coordinate system is notated  $xyz$ , four Cluster spacecraft are notated C1, C2, C3 and C4.

We selected current sheets from 221 pristine solar wind intervals from 35 days in 2003–2004 (Table 1). The list of the intervals can be found in Supporting Materials (SM). A solar wind interval was considered pristine that is not affected by the Earth’s bow shock if the electric field spectrum exhibited only electric field fluctuations at local plasma frequency and possibly its harmonics. Visually inspecting electron and proton pitch-angle distributions from a few tens of eV to about 30 keV, we assured the absence of electron and ion beams typical of foreshock. Table 1 presents typical values of background plasma parameters for each day along with maximum and minimum spatial separations between Cluster spacecraft. Note that Cluster spacecraft were separated by either less than 300 km or more than about 3,000 km.

The selection procedure of current sheets was based on a single-spacecraft Partial Variance of Increments (PVI) method, which allows identifying coherent structures by highlighting sharp gradients in the magnetic field compared to the background [23, 61]. The selection procedure was essentially equivalent to those used previously [10, 12, 13], but PVI indexes were computed for various time increments  $\tau$ , rather than only the increment dictated by data resolution.

We recall that  $PVI_\tau(t) = (\sum_\alpha \Delta B_\alpha^2(t, \tau) / \sigma_\alpha^2)^{1/2}$ , where  $\Delta B_\alpha(t, \tau) = B_\alpha(t + \tau) - B_\alpha(t)$  are increments of three magnetic field components ( $\alpha = x, y, z$ ) and  $\sigma_\alpha$  is a standard deviation of  $\Delta B_\alpha(t, \tau)$  computed over 2h intervals, a few outer correlation scales of solar wind turbulence [62]. We used magnetic field measurements aboard C4 to compute PVI indexes at time increments  $\tau = 1/22, 4/22, 16/22, 1, 4, 16, 64$ s, which allows identifying coherent structures of different scales. Each cluster of points satisfying  $PVI_\tau > 5$  was encompassed by a 3 second to 3 minute interval depending on the time increment  $\tau$  and the maximum variance component of the magnetic field computed by MVA for that interval was visually inspected [63]. Note that merging of overlapping intervals and exclusion of those nested into others have substantially reduced the required visual inspection. For all intervals with the maximum variance component reversing sign we manually adjusted current sheet boundaries, that is the regions to the left and right of the magnetic field reversal. Each current sheet identified aboard C4 was also observed aboard other Cluster spacecraft, though a few tens of current sheets had to be excluded because the magnetic field profile observed aboard one of the other spacecraft was not correlated well enough with the magnetic field profile observed aboard C4. The final dataset includes 2,033 current sheets observed aboard four Cluster spacecraft (Table 1).

Figure 1 presents an overview of the longest interval from our dataset, encompassing February 12 and 13, 2003. Panels (a)–(c) present the magnetic field, plasma density and flow velocity observed aboard C4. The magnetic field magnitude was 2–10 nT, the plasma density and proton flow velocity were respectively around 10–20  $\text{cm}^{-3}$  and 350 km/s through the entire interval. The electric field spectrum in panel (d) indicates that Cluster was in a pristine solar wind, since electric field fluctuations were only observed at local electron plasma frequency and its second harmonic. PVI indexes computed at several time increments,  $\tau = 1/22, 1$  and 64s, are presented in panels (e)–(g). In accordance with higher intermittency at smaller scales [64], we observe higher occurrence of  $PVI_\tau > 5$  at smaller time increments. This indicates higher occurrence of smaller scale coherent structures in the solar wind. Also in accordance with previous observations [65], small-scale coherent structures are typically around large-scale coherent structures. Because of that almost all current sheets are already identified by  $PVI_\tau > 5$  at several smallest time increments.

Figure 2 presents a current sheet (CS) observed around 06:10 UT on February 13, 2003 to demonstrate our methodology. Panel (a) presents the magnetic field component  $B_L$  observed aboard individual Cluster spacecraft. Note that  $\mathbf{L} \approx (0.58, -0.16, 0.80)$  is the optimal maximum variance vector, that is a unit vector with the least angular deviation from four maximum variance vectors estimated by applying MVA to magnetic field measurements of individual Cluster spacecraft. The maximum angle between individual maximum variance vectors of  $\alpha_{LL} \approx 2^\circ$  indicates a local CS planarity. Applying timing or triangulation technique [1, 47, 48, 66], which uses time delays between the occurrence of the CS aboard individual Cluster spacecraft, we estimate the local CS normal and its propagation velocity along the normal in the spacecraft frame. The revealed timing normal  $\mathbf{N}_T = (-0.77, -0.40, 0.49)$  is almost perpendicular to the optimal maximum variance vector  $\mathbf{L}$  with corresponding angle of  $\alpha_{NL} \approx 88^\circ$ , which is another indication of the local CS planarity. The angle  $\alpha_{\max} = \max(\alpha_{LL}, |90^\circ - \alpha_{NL}|) \approx 2^\circ$  can be considered a quantitative indicator of CS planarity on the scale of Cluster spacecraft separation. The revealed CS propagation velocity  $V_N \approx 284$  km/s is quite consistent with the normal component of the ion flow velocity  $V_{iN} \equiv \mathbf{V}_i \cdot \mathbf{N}_T \approx 297$  km/s, which reflects the validity of the Taylor hypothesis.

Applying MVA to magnetic field measurements of individual Cluster spacecraft we computed four minimum variance vectors. We only use minimum variance vector  $\mathbf{N}_{MVA} = (0.40, -0.79, -0.47)$  revealed aboard C4, but the use of the other normal vectors results in essentially identical results (not shown). The eigenvalues corresponding to maximum, intermediate and minimum variance vectors were  $(\lambda_{\max}, \lambda_{\text{int}}, \lambda_{\text{min}}) \approx (4, 0.04, 0.01)$ . The minimum

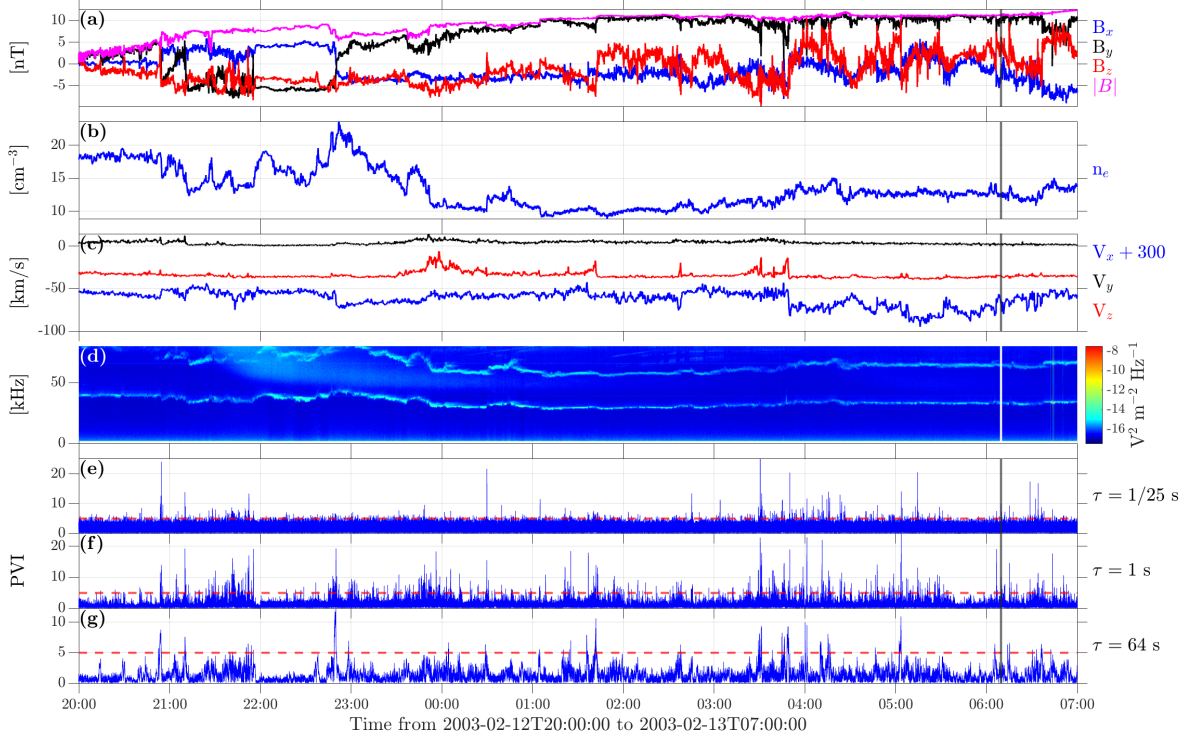


Figure 1: Overview of Cluster observations in a pristine solar wind interval extending from February 12, 2003 to the next day. Panels (a)–(c) present C4 measurements of the magnetic field measured at 22 Samples/s resolution, electron density and flow velocity at 8s cadence, and electric field spectra at about 0.1s cadence; all vector quantities are in the Geocentric Solar Ecliptic (GSE) coordinates. Panels (e)–(g) demonstrate PVI indexes computed at time increments  $\tau = 1/22$ , 1 and 64s. Current sheets were collected by inspecting magnetic field fluctuations with PVI indexes above the threshold of  $PVI_\tau = 5$  shown by red dashed lines. The vertical line around 06:10 UT on February 13 indicates the occurrence time of the current sheet shown in Figure 2.

variance vector  $\mathbf{N}_{MVA}$  is almost perpendicular to the timing normal  $\mathbf{N}_T$ , the corresponding angle is about  $110^\circ$ . This analysis demonstrates that MVA is *highly inaccurate* in estimating the CS normal in spite of relatively high ratio between intermediate and minimum eigenvalues,  $\lambda_{int}/\lambda_{min} \approx 4$ . In contrast, the cross-product of averaged magnetic fields at the CS boundaries delivers vector  $\mathbf{N}_X = (-0.77, -0.37, 0.52)$  that is consistent with the timing normal  $\mathbf{N}_T$  within about  $2^\circ$ .

The magnetic field in panel (b) is presented in a local CS coordinate system LMN, where  $\mathbf{M} = \mathbf{N}_T \times \mathbf{L}$  is the guide field direction, while the maximum variance vector  $\mathbf{L}$  was corrected,  $\mathbf{L} \rightarrow \mathbf{L} - \mathbf{N}_T (\mathbf{L} \cdot \mathbf{N}_T)$ , to make it strictly perpendicular to the timing normal and normalized to unity. Note that, in principle, we could correct the timing normal instead of the maximum variance vector. The magnetic field magnitude was around 11 nT across the CS, while the normal component  $B_N$  was only about 0.1 nT within the CS. The revealed normal component of 0.1 nT is however within the methodology uncertainty of  $11 \text{ nT} \cdot \sin \alpha_{max} \approx 0.4 \text{ nT}$  resulting from the angular uncertainty  $\alpha_{max} \approx 2^\circ$  of the maximum variance vector and timing normal. This angular uncertainty results from the fact that we could, in principle, correct the timing normal to make it perpendicular to the optimal maximum variance vector and also use the maximum variance vectors observed aboard individual Cluster spacecraft rather than the optimal vector  $\mathbf{L}$  (SM). The current sheet is therefore either a tangential discontinuity or rotational discontinuity with the normal component within the methodology uncertainty of 0.4 nT. Importantly, the use of minimum variance vector  $\mathbf{N}_{MVA}$  for the CS normal would overestimate the normal component by a factor of hundred, since MVA basically confuses the normal and guide field directions for this CS.

We use the propagation velocity of the CS to translate its temporal magnetic field profile into spatial one and also compute the current density presented in panel (c):  $J_M = -(\mu_0 V_N)^{-1} dB_L/dt$  and  $J_L = (\mu_0 V_N)^{-1} dB_M/dt$ , where  $\mu_0$  is the vacuum permeability and the time step is dictated by data resolution,  $dt = 1/22 \text{ s}$ . Note that the curlometer technique would substantially underestimate the current density (e.g., Vasko et al., 2014 [67]), because the thickness of

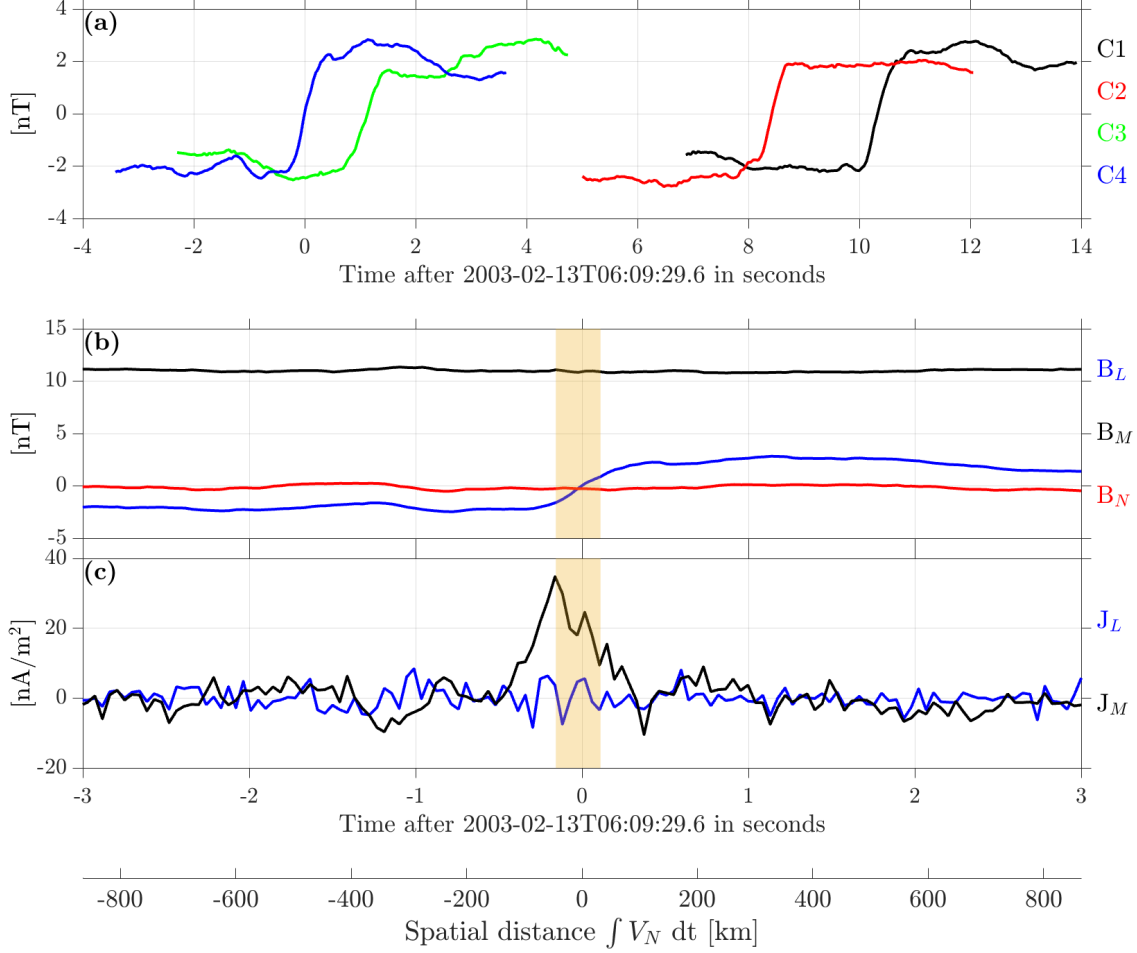


Figure 2: The current sheet observed on February 13, 2003 around 06:10 UT (Section 3): (a) the magnetic field component  $B_L$  observed aboard C1–C4 at 25 Samples/s resolution, where  $\mathbf{L}$  is the optimal maximum variance direction of the magnetic field; (b) three magnetic field components observed aboard C4 in the local coordinate system;  $B_L$  is the maximum variance component,  $B_M$  and  $B_N$  are guide field and normal components; (c) current density components computed using the current sheet propagation velocity  $V_N$  revealed by the timing method,  $J_M = -(\mu_0 V_N)^{-1} dB_L/dt$  and  $J_L = (\mu_0 V_N)^{-1} dB_M/dt$ , where the time step is dictated by data resolution,  $dt = 1/22$  s. The CS central region is highlighted in panels (b) and (c) and corresponds to  $|B_L - \langle B_L \rangle| \leq 0.25 \Delta B_L$ , where  $\Delta B_L$  is the variation of  $B_L$  between the boundaries and  $\langle B_L \rangle$  is the mean of  $B_L$  values at the CS boundaries. The bottom axis converts temporal scale of the current sheet into spatial scale by multiplying with the revealed propagation velocity.

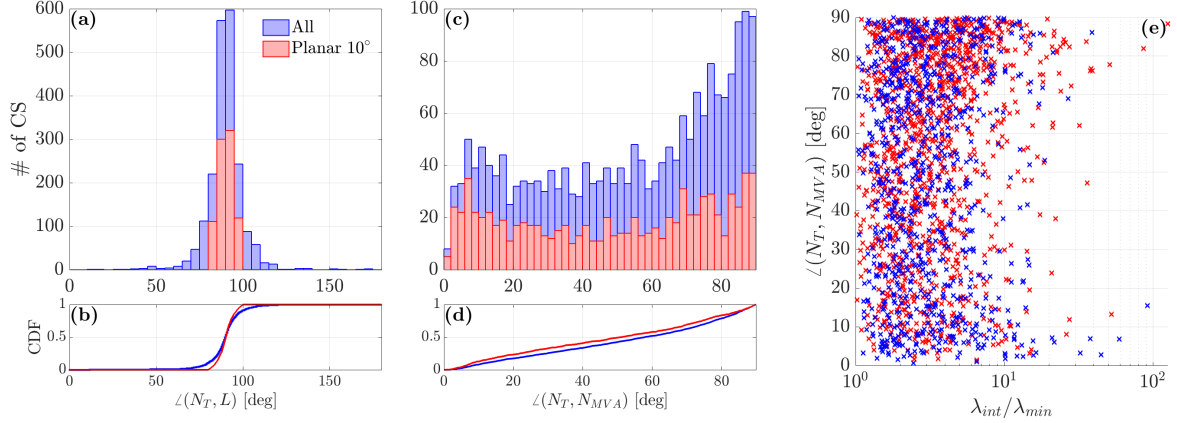


Figure 3: The demonstration of planarity of the CSs and MVA inaccuracy in estimating the CS normal (Section 4). Panels (a) and (b) present probability and cumulative distributions of the angle between optimal maximum variance vector  $\mathbf{L}$  and timing normal  $\mathbf{N}_T$ . Panels (c) and (d) show probability and cumulative distributions of the angle between timing normal  $\mathbf{N}_T$  and minimum variance vector  $\mathbf{N}_{MVA}$  computed for the magnetic field measured aboard C4. Panel (e) demonstrates a scatter plot of the angle between  $\mathbf{N}_{MVA}$  and  $\mathbf{N}_T$  versus the ratio  $\lambda_{int}/\lambda_{min}$  between intermediate and minimum eigenvalues that is supposed to be a theoretical indicator of MVA accuracy. The distributions and data shown by different colors correspond to all CSs and CSs of sufficiently high planarity with  $\alpha_{max} \leq 10^\circ$ .

solar wind CSs is typically smaller than Cluster spacecraft separation [8, 12, 13]. The CS half-thickness is estimated as  $\lambda = \Delta B_L / 2\mu_0 \langle J_M \rangle$ , where  $\Delta B_L$  is the variation of  $B_L$  between the CS boundaries and  $\langle J_M \rangle$  is the current density averaged over the CS central region. The latter is highlighted in the panels and corresponds to  $|B_L - \langle B_L \rangle| \leq 0.25\Delta B_L$ , where  $\langle B_L \rangle$  is the mean of  $B_L$  values at the CS boundaries and the factor of 0.25 has been chosen to have at least three data points in the central region for all the CSs in our dataset. Since solar wind CSs are predominantly magnetic field rotations and the current density is dominated by the component parallel to local magnetic field [8, 12, 13], we characterize each CS by the parallel current density averaged over the CS central region,  $J_0 \equiv \langle J_{||} \rangle$  and shear angle  $\Delta\theta$  between magnetic fields at the CS boundaries. We found that the considered CS is a proton kinetic-scale structure with half-thickness  $\lambda \approx 65$  km that is around  $\lambda_p$  in units of local proton inertial length. The averaged parallel current density  $J_0 \approx 24$  nA/m<sup>2</sup> is around  $0.2J_A$ , where  $J_A = en_i V_A$  is local Alfvén current density and  $V_A$  is local Alfvén speed. Both proton inertial length and Alfvén current density are so-called Alfvén units typically used in turbulence simulations [44, 45, 32].

We carried out similar analysis for all the collected 2,033 CSs. We obtained single-spacecraft estimates of the half-thickness and current density notated respectively  $\lambda^*$  and  $J_0^*$ . In the single-spacecraft methodology that was applied to C4 measurements the maximum variance vector is still delivered by MVA, but the CS normal is determined by the cross-product method and the propagation velocity is assumed to coincide with the normal component of local ion flow velocity [8, 38, 13]. Single-spacecraft estimates ( $\lambda^*$  and  $J_0^*$ ) will generally differ from four-spacecraft estimates ( $\lambda$  and  $J_0$ ) because the normal and propagation velocity are computed differently. Note that for 28 CSs the magnetic field profile was bifurcated and the current sheet thickness and current density were not computed, because the current density  $\langle J_M \rangle$  averaged over the central region of a bifurcated CS is close to zero and the estimate  $\Delta B_L / 2\mu_0 \langle J_M \rangle$  does not reflect the actual CS thickness [12]. These CSs were only excluded from the analysis of the current sheet thickness and current density amplitude in Figure 9. In the next section we quantify the accuracy of the different methods in estimating the actual CS normal and also the accuracy of the single-spacecraft methodology in estimating the CS properties.

## 4 MVA and recommended single-spacecraft methodology

Figure 3 presents the analysis of MVA accuracy in estimating the actual CS normal. Importantly, the actual CS normal is not known exactly, since the timing normal has uncertainties associated at least with the degree of CS planarity on the scale of Cluster spacecraft separation. The analysis of the CSs of sufficiently high planarity allows however improving the alignment of the timing normal with the actual CS normal. Panels (a) and (b) present probability and corresponding cumulative distributions of the angle  $\alpha_{NL}$  between the optimal maximum variance vector  $\mathbf{L}$  and the timing normal  $\mathbf{N}_T$ . Typically the two vectors are almost perpendicular as it should be for locally planar structures.

We also demonstrate in panels (a) and (b) similar distributions for CSs of different degree of planarity quantified by  $\alpha_{\max} = \max(|90^\circ - \alpha_{NL}|, \alpha_{LL})$ , where we recall that  $\alpha_{LL}$  is the maximum angle between maximum variance vectors observed aboard individual Cluster spacecraft. Not surprisingly the distribution of  $\alpha_{NL}$  is more narrow around  $90^\circ$  for the CSs of higher planarity. Panels (c) and (d) present probability and cumulative distributions of the angle between the minimum variance vector  $\mathbf{N}_{MVA}$  observed aboard C4 and the timing normal  $\mathbf{N}_T$ ; the use of minimum variance vectors observed aboard other Cluster spacecraft would result in similar statistical distributions (not shown). The MVA turns out to be *highly inaccurate* in estimating the CS normal, since the minimum variance vector is typically highly oblique to the timing normal. The corresponding angle is often around  $90^\circ$  and larger than  $60^\circ$  for about 50% of the CSs. The MVA accuracy is not strongly dependent on the degree of local CS planarity, since probability and cumulative distributions for the CSs with  $\alpha_{\max} \leq 10^\circ$  are essentially identical. Even more surprising panel (e) shows that the MVA accuracy is not correlated with the ratio  $\lambda_{\text{int}}/\lambda_{\text{min}}$  between intermediate and minimum eigenvalues that is theoretically supposed to indicate MVA accuracy or at least be a requirement for accuracy [68, 63].

Figure 4 presents the analysis of MVA accuracy dependence on the separation between Cluster spacecraft. Panels (a) and (b) show probability distributions of the angle between  $\mathbf{N}_{MVA}$  and  $\mathbf{N}_T$  for the CSs of high planarity,  $\alpha_{\max} \leq 10^\circ$ , but observed in the intervals, when the maximum spatial separation between Cluster spacecraft was either less than 300 km or larger than 3,000 km. Along with the corresponding cumulative distributions in panels (c) these probability distributions show that MVA inaccuracy is independent of the spatial separation between Cluster spacecraft. This statement is also corroborated by the analysis of all the CSs, rather than only those of sufficiently high planarity (SM). We speculate on the cause of the revealed MVA inaccuracy in Section 5.

Figure 5 demonstrates probability and cumulative distributions of the angle between the cross-product vector  $\mathbf{N}_X$  and the timing normal  $\mathbf{N}_T$ . The angle is within  $20^\circ$  for about 80% of the CSs and the agreement is even better for the CSs of higher planarity. This better agreement results from a lower uncertainty of the timing normal for the CSs of higher planarity. The higher the planarity the more accurately the timing normal aligns with the actual CS normal and the better is the alignment between the timing normal and the cross-product vector. The fact that the cross-product vector delivers a reasonable estimate of the actual CS normal implies that the normal magnetic field component across the CSs is typically small compared to the guide field. The distribution of the angle between  $\mathbf{N}_X$  and  $\mathbf{N}_T$  for the CSs with  $\alpha_{\max} \leq 10^\circ$  demonstrates that the cross-product method is rather accurate in estimating the actual CS normal; its angular uncertainty is within  $15^\circ$  ( $10^\circ$ ) at the confidence level of 90% (75%).

Figure 6 presents the comparison between local ion flow velocity along the timing normal  $V_{iN}$  and the CS propagation velocity  $V_N$  revealed by the timing method. Panels (a) and (b) show that the two velocities are typically consistent and agree even better for the CSs of higher planarity. Panel (c) shows  $V_N$  and  $V_{iN}$  are consistent within 20% for more than 90% of the CSs with  $\alpha_{\max} \leq 10^\circ$ . The better agreement between  $V_N$  and  $V_{iN}$  is certainly due to a lower uncertainty of the timing normal for the CSs of higher planarity. Thus, the Taylor hypothesis is statistically valid for CSs in the solar wind.

Figure 7 presents the comparison of the half-thickness  $\lambda$  and current density amplitude  $J_0$  obtained using the four-spacecraft methodology (Figures 2) with corresponding estimates  $\lambda^*$  and  $J_0^*$  revealed by the single-spacecraft methodology based on the cross-product normal and frozen-in assumption. The four-spacecraft estimates have uncertainties associated with the degree of CS planarity on the scale of Cluster spacecraft separation, but these uncertainties are reduced by considering the CSs of sufficiently high planarity. Panels (a) and (b) demonstrate the ratio between four- and single-spacecraft estimates for the CSs with different  $\alpha_{\max}$ . The probability and cumulative distributions for the CSs with  $\alpha_{\max} \leq 10^\circ$  demonstrate that the single-spacecraft methodology is quite accurate in estimating the CS thickness and current density amplitude. For more than about 90% of the CSs with  $\alpha_{\max} \leq 10^\circ$  we have  $0.8 \lesssim \lambda^*/\lambda \lesssim 1.2$  and  $0.8 \lesssim J_0^*/J_0 \lesssim 1.2$ . Thus, the single-spacecraft methodology based on the cross-product normal and frozen-in assumption delivers CS thickness and current density estimates with accuracy of better than 20% at the confidence level of 90%.

## 5 Nature and properties of the current sheets

Since solar wind CSs have negligible variations of the magnetic field magnitude [8, 12], whether a CS is a tangential or rotational discontinuity is determined solely by the magnitude of the normal magnetic field component. Note that the Wälén relation well satisfied across solar wind CSs [50, 51, 52] is not a unique feature of rotational discontinuities, since tangential discontinuities are not prohibited to satisfy it too [49]. The normal component  $B_N$  may be however within methodology uncertainty because of the angular uncertainty  $\alpha_{\max}$  of the timing normal. Indeed, the timing normal is not likely to be strictly aligned with the actual CS normal and a significant fraction of the magnetic field component along the timing normal can be due to the projection of the actual guide field onto that normal. Because of the angular uncertainty, a finite component will be always observed along the timing normal even for tangential discontinuities.

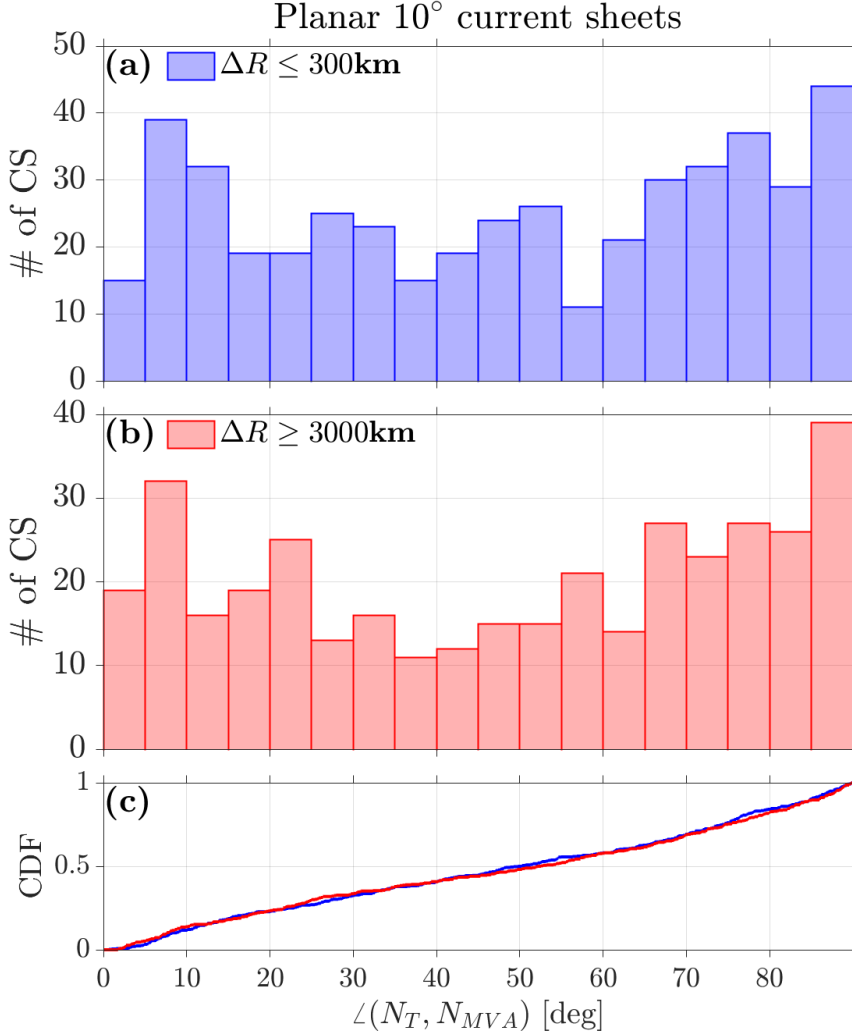


Figure 4: The demonstration that MVA accuracy is independent of the maximum spatial separation between Cluster spacecraft: (a,b) probability distributions of the angle between the minimum variance vector  $N_{MVA}$  and the timing normal  $N_T$  for the CSs of high planarity,  $\alpha_{\max} \leq 10^\circ$ , but observed in the intervals, when the maximum spatial separation between Cluster spacecraft was either less than 300 km or larger than 3,000 km; (c) cumulative distribution functions corresponding to the probability distributions.

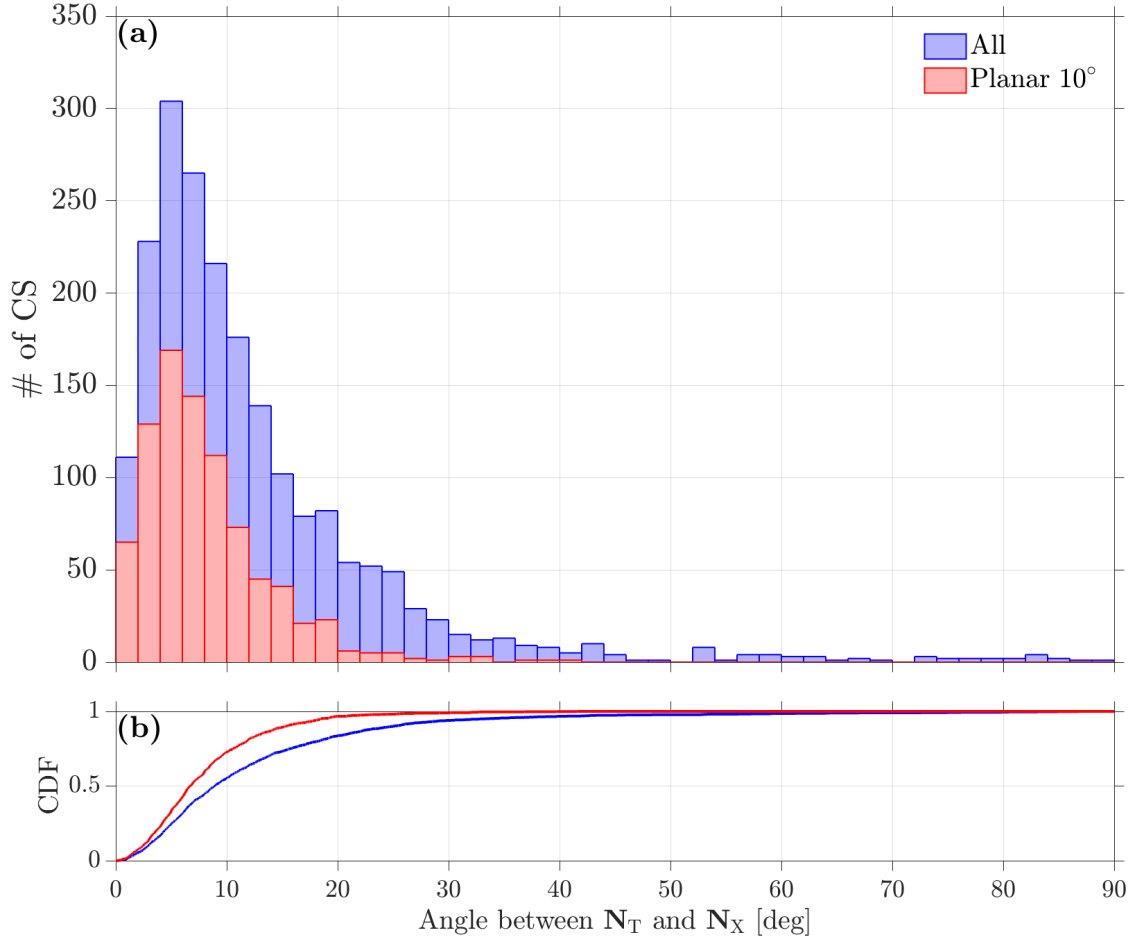


Figure 5: The probability and cumulative distributions of the angle between timing normal  $\mathbf{N}_T$  and the cross-product vector  $\mathbf{N}_X$  that is a unit vector along the cross-product of magnetic fields at the CS boundaries. The distributions of different colors correspond to all CSs and CSs of sufficiently high planarity with  $\alpha_{\max} \leq 10^\circ$ .

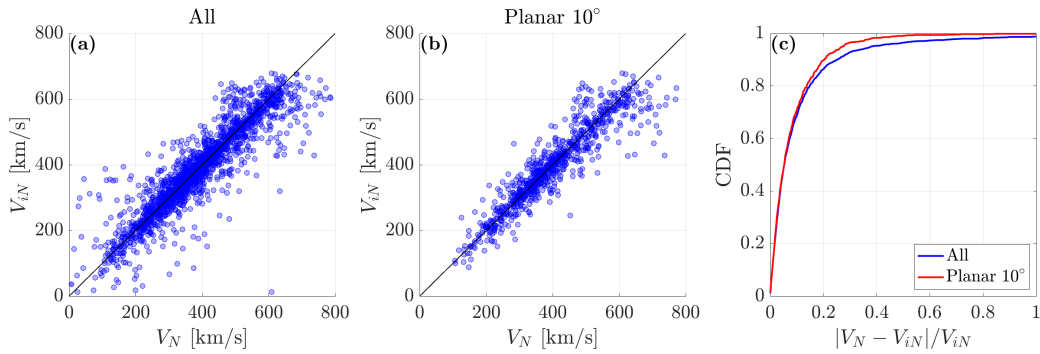


Figure 6: The comparison between the CS propagation velocity  $V_N$  revealed by the timing method and local ion flow velocity  $V_{iN}$  along the timing normal. Panels (a) and (b) present scatter plots of  $V_{iN}$  vs.  $V_N$  for all CSs and CSs of sufficiently high planarity with  $\alpha_{\max} \leq 10^\circ$ , while panel (c) demonstrates corresponding cumulative distributions of  $|V_N - V_{iN}|/V_{iN}$ .

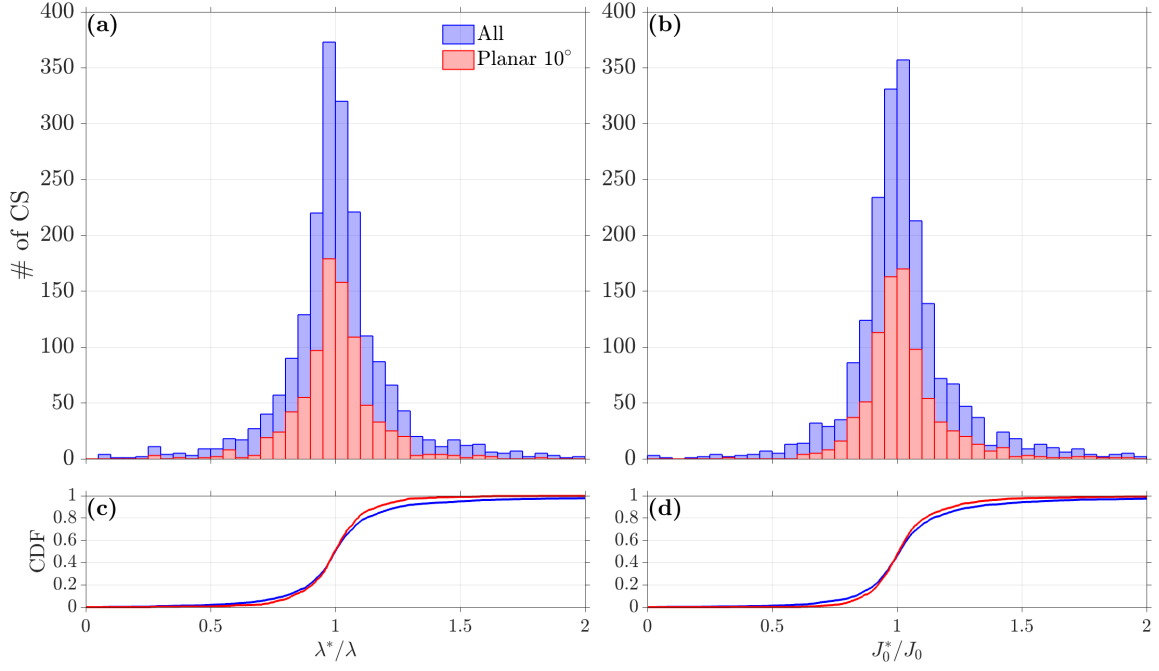


Figure 7: The comparison between single-spacecraft and multi-spacecraft estimates of the CS thickness and current density. Single-spacecraft estimates  $\lambda^*$  and  $J_0^*$  were obtained by computing the CS normal using the cross-product method and assuming that the CSs are frozen into local plasma flow (Taylor hypothesis). Multi-spacecraft estimates  $\lambda$  and  $J_0$  were obtained using the CS normal and propagation velocity estimated by the timing method. The distributions of different colors correspond to all CSs and CSs of sufficiently high planarity with  $\alpha_{\max} \leq 10^\circ$

The nature of the CSs can be addressed by comparing the observed normal component  $B_N$  with  $\langle B \rangle \sin \alpha_{\max}$ , where here and below  $B_N$  and  $\langle B \rangle$  are averaged values of the normal component and magnetic field magnitude over the CS central region. Note that  $\langle B \rangle \sin \alpha_{\max}$  is the maximum value of the magnetic field component along the timing normal that would be observed across perfect tangential discontinuities because of the angular uncertainty  $\alpha_{\max}$  of the timing method (SM).

Figure 8 presents the analysis of the normal magnetic field component for all the collected 2,033 CSs. Panel (a) compares  $B_N/\langle B \rangle$  and  $\sin \alpha_{\max}$  and demonstrates that about 96% of the CSs have the normal component within the uncertainty,  $B_N \lesssim \langle B \rangle \sin \alpha_{\max}$ . Thus, these CSs can be either tangential discontinuities or rotational discontinuities, whose normal component is within the methodology uncertainty. About 4% of the CSs with  $B_N \gtrsim \langle B \rangle \sin \alpha_{\max}$  could be interpreted in terms of rotational discontinuities if the angular uncertainty was the only uncertainty of the timing method. There is however an additional uncertainty caused by uncertainties of the time delays between the occurrence of the same CS aboard different Cluster spacecraft (Figure 2a). In the timing method we used time delays delivering the maximum cross-correlation between magnetic field profiles observed aboard different Cluster spacecraft, but each time delay has an uncertainty determined by the broadness of the cross-correlation function. We estimated uncertainties of the normal component caused by the uncertainty of the time delays for the CSs with  $B_N \gtrsim \langle B \rangle \sin \alpha_{\max}$  (SM). Panel (b) presents the estimated uncertainties and demonstrates that a substantial fraction of this 4% of the CSs may actually have  $B_N \lesssim \langle B \rangle \sin \alpha_{\max}$ , because of the relatively large uncertainty caused by the time delay uncertainties. Only half of those CSs or, equivalently, less than 2% of the entire dataset have  $B_N \gtrsim \langle B \rangle \sin \alpha_{\max}$ . Thus, even four-spacecraft measurements do not allow us to classify the majority of the CSs in terms of tangential or rotational discontinuities.

Figure 9 presents the properties of all the collected CSs, except 28 bifurcated ones. We present single-spacecraft estimates  $\lambda^*$  and  $J_0^*$ , since in contrast to multi-spacecraft estimates  $\lambda$  and  $J_0$  their uncertainty is independent of CS planarity as well as time delay uncertainties. Panels (a) and (b) demonstrate that the CSs have half-thickness from a few tens to a few thousand kilometers and current density amplitude from about a few to a few tens of  $\text{nA/m}^2$ . The most typical values of the CS half-thickness and current density are around 100 km and  $5 \text{ nA/m}^2$ , respectively. Panels (c) and (d) present the CS half-thickness and current density in local Alfvén units and demonstrate that the CSs are proton

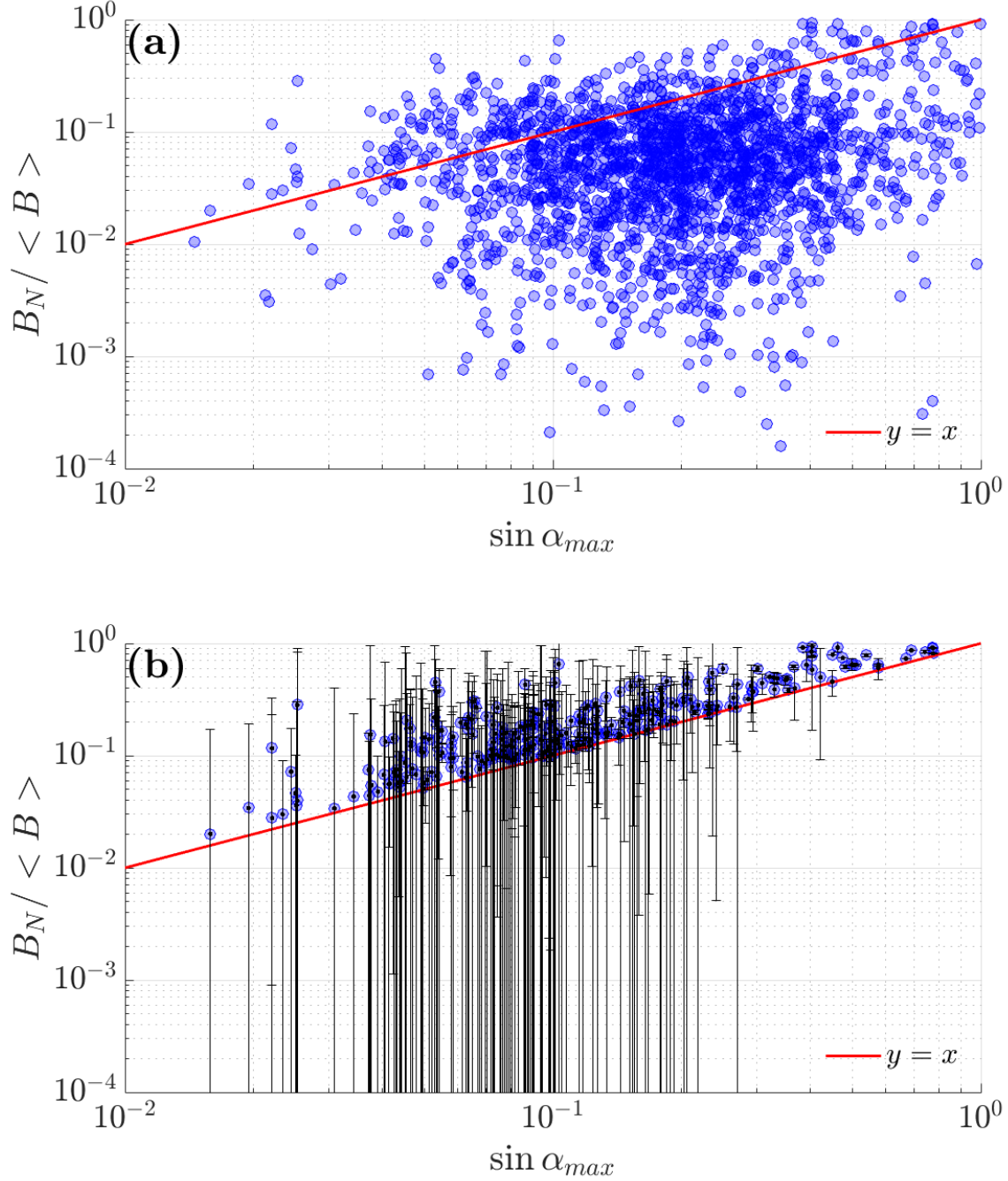


Figure 8: The analysis of the magnetic field component along the timing normal: (a) a scatterplot of  $B_N / \langle B \rangle$  versus its uncertainty  $\sin \alpha_{max}$  determined by the degree of CS planarity on the scale of Cluster spacecraft separation, where both the normal component  $B_N$  and magnetic field magnitude  $\langle B \rangle$  were averaged over the CS central region; (b)  $B_N / \langle B \rangle$  versus  $\sin \alpha_{max}$  for the CSs with  $B_N \gtrsim \langle B \rangle \sin \alpha_{max}$ , where error bars indicate the uncertainty caused by the uncertainty of the time delays used in the timing method (Section 5).

kinetic-scale structures with current density amplitudes within a few tenths of local Alfvén current density. The most typical values of the CS half-thickness and current density amplitude are around  $1.5\lambda_p$  and  $0.05J_A$ , respectively. Panels (e) and (f) demonstrate that the shear angle  $\Delta\theta$  and normalized current density  $J_0^*/J_A$  are correlated with normalized half-thickness  $\lambda^*/\lambda_p$ . These scale-dependencies are revealed by bin median profiles as well as by power-law fits shown in the panels. The shear angle tends to be larger for larger-scale CSs,  $\Delta\theta \approx 13.6^\circ (\lambda^*/\lambda_p)^{0.5}$ , while the current density amplitude tends to be larger for smaller-scale CSs,  $J_0^*/J_A \approx 0.12 \cdot (\lambda^*/\lambda_p)^{-0.5}$ . Note that the scale-dependence of the current density could be deduced from the scale-dependence of the shear angle, since  $J_0^* \approx \langle B \rangle \Delta\theta / 2\mu_0 \lambda$  or, equivalently,  $J_0^*/J_A \approx \Delta\theta \cdot (2\lambda/\lambda_p)^{-1}$ . These scale-dependencies and CS properties are discussed in the next section.

## 6 Discussion

The majority of studies of solar wind current sheets were performed using single-spacecraft measurements and relied on the normal estimates by MVA [3, 5, 6, 7, 69]. Four-spacecraft analysis of solar wind CSs by Knetter et al., 2004 [48] demonstrated however that MVA is not accurate in estimating the CS normal and the most accurate single-spacecraft estimate is delivered by the cross-product of magnetic fields at the CS boundaries. For that reason the recent statistical studies of magnetic reconnection [38, 39, 35, 40] and CSs in general [8, 12, 13, 14] observed at 1 AU as well as near the Sun have been based on the cross-product normals. In this paper we have substantially expanded the previous multi-spacecraft studies of solar wind CSs using a dataset of more than two thousand CSs observed aboard four Cluster spacecraft. Our dataset is a factor of ten larger than the dataset of about a hundred CSs considered by Knetter et al., 2004 [48] and includes CSs from 35 days, when the Cluster spacecraft were separated by either about 300 or 3,000 km (Table 1). Four-spacecraft observations allowed us to estimate the CS normal and other CS properties using the timing method, while their comparison to different single-spacecraft estimates allowed revealing the accuracy of the latter. Note that the timing method has uncertainty determined by the CS planarity on the scale of Cluster spacecraft separation, but considering CSs of sufficiently high planarity allowed us to reduce this uncertainty. The use of the extensive dataset allows achieving statistical validity of all our conclusions.

We showed that MVA is indeed *highly inaccurate* in estimating the normal to CSs in the solar wind (Figure 4). Surprisingly, the minimum variance direction that is supposed to deliver the normal is often highly-oblique to the actual CS normal and, hence, more aligned with the actual guide field direction. Even more surprising is that the MVA accuracy is not correlated with the ratio  $\lambda_{\text{int}}/\lambda_{\text{min}}$  between intermediate and minimum variances that is supposed to be a theoretical indicator of MVA accuracy. Importantly, the fundamental assumption of the MVA method is that the noise (instrumental or natural) is isotropic [68, 63]. Only in that case the CS normal and guide field directions are delivered by respectively minimum and intermediate variance directions, while the ratio  $\lambda_{\text{int}}/\lambda_{\text{min}}$  indicates the MVA accuracy. However, magnetic field fluctuations within and around CSs (the natural noise from the MVA perspective) are not isotropic, since solar wind turbulence is generally anisotropic. The magnetic field fluctuations in solar wind turbulence tend to be perpendicular to local magnetic field,  $\delta B_\perp^2 \gg \delta B_\parallel^2$  [70, 71, 72]. For that reason a CS with a small normal component (say, a perfect tangential discontinuity) immersed into solar wind turbulence may have the minimum variance along background magnetic field that is mostly along the guide field direction, rather than the actual CS normal. Thus, because of the natural anisotropy of solar wind turbulence the minimum variance direction delivered by MVA can be highly oblique to the actual CS normal in accordance with observations (Figure 4). In turn, MVA accuracy is not correlated with  $\lambda_{\text{int}}/\lambda_{\text{min}}$  (Figure 4), because variances  $\lambda_{\text{int}}$  and  $\lambda_{\text{min}}$  are dominated by ambient anisotropic magnetic field fluctuations. Note that we also tried to apply MVA only to the magnetic field at the CS boundaries, rather than to the entire CS transition region, but we observed no improvement of the MVA accuracy (not shown).

Since MVA is highly inaccurate in the solar wind, we agree with Knetter et al., 2004 [48] and Neugebauer et al., 2006 [49] that the previous classifications of solar wind CSs in terms of tangential or rotational discontinuities based on the magnetic field component along the MVA normal are not reliable [3, 5, 6, 7]. The same statement is also relevant to the recent classification of solar wind current sheets [69] and current layers at the boundaries of switchbacks observed in the near-Sun solar wind [73, 74, 75]. In fact, even four-spacecraft observations do not allow us to confidently classify the current sheets in terms of tangential or rotational discontinuities. Note that the Wálen relation well satisfied across solar wind CSs [50, 51, 52] is not a unique feature of rotational discontinuities, since tangential discontinuities are not prohibited to satisfy it too [49]. Thus, the classification of solar wind currents sheets in terms of tangential and rotational discontinuities remains a challenge.

We demonstrated that the cross-product of magnetic fields at the CS boundaries delivers an accurate estimate of the actual CS normal that is in accordance with the analysis by Knetter et al., 2004 [48]. The angular uncertainty of the cross-product method is less than  $15^\circ$  ( $10^\circ$ ) at the confidence level of at least 90% (75%) (Figure 5). This high precision of the cross-product method implies that the normal component is typically much smaller than the guide field component. We also demonstrated that the Taylor frozen-in hypothesis is statistically valid for solar wind CSs that is in accordance with previous analysis of solar wind turbulence (e.g., Chasapis et al., 2017 [76]). The CS propagation

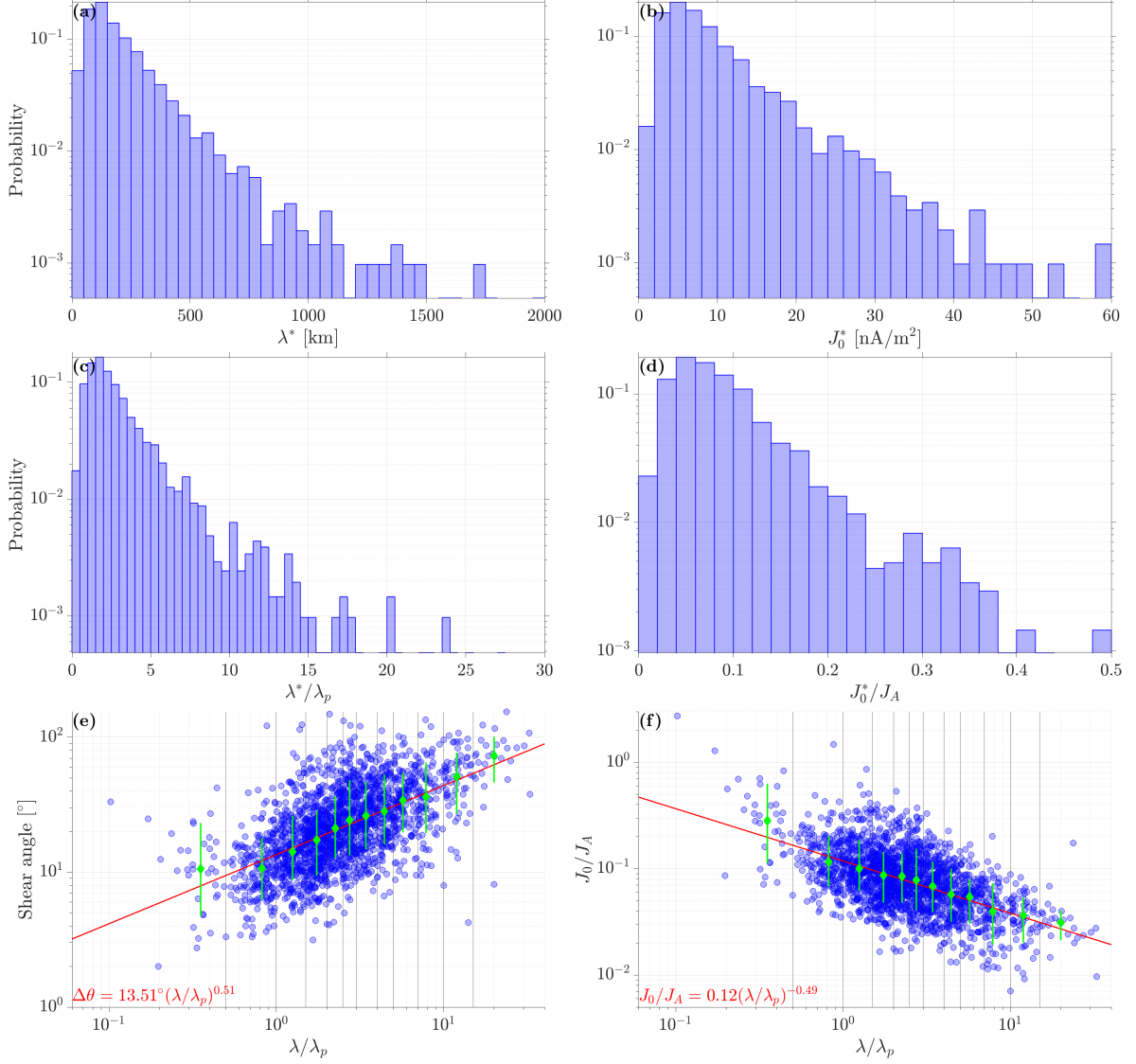


Figure 9: The properties of the collected 2,033 CSs, except 28 bifurcated ones, estimated using the single-spacecraft methodology. Panels (a) and (b) show probability distributions of the CS half-thickness  $\lambda^*$  and current density amplitude  $J_0^*$  in physical units, while panels (c) and (d) present distributions of  $\lambda^*/\lambda_p$  and  $J_0^*/J_A$ , where  $\lambda_p$  is local proton inertial length and  $J_A = en_i V_A$  is local Alfvén current density. Panels (e) and (f) demonstrate the scale-dependence of the shear angle  $\Delta\theta$  and normalized current density  $J_0^*/J_A$  on normalized CS half-thickness  $\lambda^*/\lambda_p$ . The best power-law fits (red) and bin-mean profiles (green) are indicated in the panels. The bars reflect the range where 70% of the data reside.

velocity is consistent with local ion flow velocity within about 20% at the 90% confidence level (Figure 6). The single-spacecraft methodology based on the cross-product normal and frozen-in assumption has been widely used for the analysis of current sheets [8, 12, 13, 14] and magnetic reconnection [38, 39, 53, 35, 40] in the solar wind. We showed that this single-spacecraft methodology is actually accurate in estimating the CS thickness and current density amplitude; it delivers the CS properties within 20% of their actual values at the confidence level of 90% (Figure 7). This result should be valuable for the analysis of current sheets near the Sun and beyond 1 AU, where only single-spacecraft measurements are available. The only unavoidable feature of this methodology is that it does not allow classifying CSs in terms of tangential or rotational discontinuities, because the normal component along the cross-product normal is by definition zero.

The collected CSs are proton kinetic-scale structures with half-thickness from a fraction to about ten proton inertial lengths and current density amplitude typically around 5% of local Alfvén current density. The most typical values of the half-thickness and current density for the CSs at 1 AU are around 100 km and 5 nA/m<sup>2</sup>, which is consistent with previous reports [10, 12, 13]. We also revealed that the shear angle and current density amplitude scale with thickness,  $\Delta\theta \approx 13.6^\circ (\lambda^*/\lambda_p)^{0.5}$  and  $J_0^*/J_A \approx 0.12 \cdot (\lambda^*/\lambda_p)^{-0.5}$ . Similar properties and almost identical scale-dependencies were reported for a larger dataset of CSs observed at 1 AU aboard Wind spacecraft [12, 13]. The scale-dependencies were shown to be a strong evidence supporting the hypothesis that the CSs are produced by turbulence cascade [13]. The other evidence supporting this hypothesis is the similarity between distributions of waiting times of CSs observed in the solar wind and numerical turbulence simulations [8, 23, 24]. The revealed CS properties in Figure 9 are basically consistent with those observed in turbulence simulations [44, 77, 32, 78], though a more detailed comparative analysis is still necessary. The fact that the normal to solar wind CSs is typically aligned with the cross-product of magnetic fields at the CS boundaries is also consistent with theory and numerical simulations that turbulence cascade produces CSs with wave vectors oriented perpendicular to background magnetic field [79, 80, 27, 31].

Even though there are several CSs in our dataset with half-thickness of  $0.1\lambda_p$ , typically the CS half-thickness is above  $0.3\lambda_p$  (Figure 9). Note that electron-scale CSs could be resolved by Cluster magnetic field measurements, since the temporal resolution of 25 S/s translates into the spatial resolution of the order of 10 km that is around  $0.1\lambda_p$ . The low occurrence of CSs thinner than about proton inertial length may indicate that CSs, whose thickness is smaller than this value, are efficiently disrupted by magnetic reconnection. This would be consistent with some turbulence and reconnection theories [81, 82]. The alternative is that electron-scale CSs are abundant in the solar wind, but did not fit our criterion of relatively stable magnetic fields at the current sheet boundaries.

## 7 Conclusion

The results of this study can be summarized as follows

1. The Minimum Variance Analysis is *highly inaccurate* in estimating the normal of current sheets in the solar wind. The minimum variance direction that is supposed to deliver the normal is often highly-oblique to the actual CS normal (the angle is larger than 60° for about 50% of the CSs) and, hence, more aligned with the actual guide field direction. We believe that the MVA inaccuracy is caused by ambient turbulent fluctuations, which are typically anisotropic.
2. The cross-product of magnetic fields at the current sheet boundaries delivers the current sheet normal with angular uncertainty of less than 15° (10°) at the confidence level of at least 90% (75%). The current sheets are essentially frozen into plasma flows, since their propagation velocity is consistent with local ion flow velocity within about 20% at the confidence level of 90%.
3. The single-spacecraft methodology based on the cross-product normal and frozen-in assumption delivers the current sheet thickness and current density amplitude within 20% of their actual values at the confidence level of 90%. This methodology will be valuable for the analysis of current sheets near the Sun and beyond 1 AU, where only single-spacecraft measurements are available.
4. Solar wind current sheets at 1 AU are proton kinetic-scale structures with the most typical half-thickness around 100 km that is around proton inertial length and the most typical current density amplitude of 5 nA/m<sup>2</sup> that is around 5% of the local Alfvén current density. Solar wind current sheets have the shear angle and current density amplitude scaling with their thickness,  $\Delta\theta \approx 13.5^\circ (\lambda/\lambda_p)^{0.5}$  and  $J_0/J_A = 0.12(\lambda/\lambda_p)^{-0.5}$ , where  $\lambda_p$  and  $J_A = en_i V_A$  are local proton inertial length and Alfvén current density.

5. The normal magnetic field component is within the methodology uncertainties and classifying solar wind current sheets in terms of tangential and rotational discontinuities remains a challenge even using multi-spacecraft measurements.

**Acknowledgments:** We would like to acknowledge Cluster Active Archive and Cluster instrument teams, in particular FGM, CIS/CODIF and CIS/HIA, Whisper for excellent data. The work of T.P. was supported by NASA Living With a Start grant No. 80NSSC20K1781. The work of F.M. was supported by NASA Heliophysics Guest Investigator grant No. 80NSSC21K0730. I.V. thanks Russian Science Foundation grant No. 21-12-00416.

Table 1: The summary of the dataset of 2,033 current sheets collected in the solar wind. For each day indicated in the first column we analyzed several time intervals (SM). The next four columns present the magnetic field magnitude  $B$ , plasma density  $n_i$ , plasma flow velocity  $V_i$ , and proton beta  $\beta_p$  all averaged over the considered time intervals. The last three columns present the maximum and minimum spatial separation ( $\Delta R_{\max}$  and  $\Delta R_{\min}$ ) between Cluster spacecraft and the number of CSs collected within the time intervals for each day.

Date	$B$ [nT]	$n_i$ [ $\text{cm}^{-3}$ ]	$V_i$ [km/s]	$\beta_p$	$\Delta R_{\max}$ [km]	$\Delta R_{\min}$ [km]	CS#
20030108	5.2	22.9	280	0.07	4815	3210	17
20030113	8.2	6.8	390	0.09	6345	2875	29
20030122	8.3	6.2	600	0.13	4205	3385	96
20030123	8.8	5.1	645	0.17	6040	2920	33
20030129	9.6	25.5	430	0.19	4110	3460	5
20030130	11.7	9.7	455	0.47	6780	3015	118
20030210	7.0	7.4	440	0.40	4230	3350	42
20030211	6.9	9.0	420	0.39	8100	3090	46
20030212	5.6	16.1	340	0.31	4800	3350	37
20030213	10.7	11.9	365	1.2	5000	3240	119
20030217	8.7	5.0	620	0.87	4000	3460	68
20030218	13.4	8.2	660	2.4	4595	3220	72
20030219	6.4	7.2	545	1.3	4910	3295	10
20030220	8.3	7.6	585	1.7	4695	3285	63
20030225	6.3	8.4	405	0.25	8245	2785	27
20030226	14.3	30.5	440	0.25	5240	3785	5
20030227	10.1	7.3	550	1.4	4330	3375	75
20030301	7.1	6.6	415	0.14	4255	3435	29
20030302	5.6	8.8	415	0.41	7630	2980	9
20030311	7.5	10.7	410	0.57	4390	3300	104
20030313	11.1	9.9	485	0.21	4015	3355	20
20030314	10.9	12.3	535	0.79	8110	2765	10
20030325	4.6	7.5	415	0.49	4495	3285	97
20030326	6.1	15.7	385	0.95	8065	2795	17
20030329	9.0	21.6	430	0.02	5105	3455	13
20030330	10.4	16.9	450	0.29	4525	3295	66
20031219	2.7	13.0	320	0.52	220	190	9
20031220	8.7	37.5	340	4.9	325	165	71
20031231	8.4	18.4	440	2.8	240	155	44
20040102	8.3	12.9	460	0.82	240	160	159
20040122	18.3	23.6	645	9.1	235	180	188
20040124	8.8	9.8	505	0.76	230	175	83
20040126	11.0	10.3	445	0.63	215	190	62
20040127	9.9	7.2	430	0.22	235	175	23
20040131	8.5	4.8	570	0.44	240	170	174

## References

- [1] Leonard F. Burlaga and Norman F. Ness. Tangential Discontinuities in the Solar Wind. *Solar Physics*, 9(2):467–477, October 1969.
- [2] F. Mariani, B. Bavassano, U. Villante, and N. F. Ness. Variations of the occurrence rate of discontinuities in the interplanetary magnetic field. *J. Geophys. Res.*, 78(34):8011, January 1973.
- [3] L. F. Burlaga, J. F. Lemaire, and J. M. Turner. Interplanetary current sheets at 1 AU. *J. Geophys. Res.*, 82:3191–3200, August 1977.
- [4] B. T. Tsurutani and E. J. Smith. Interplanetary discontinuities - Temporal variations and the radial gradient from 1 to 8.5 AU. *J. Geophys. Res.*, 84:2773–2787, June 1979.
- [5] R. P. Lepping and K. W. Behannon. Magnetic field directional discontinuities - Characteristics between 0.46 and 1.0 AU. *J. Geophys. Res.*, 91:8725–8741, August 1986.

- [6] Bruce T. Tsurutani, C. M. Ho, J. K. Arballo, E. L. Smith, B. E. Goldstein, M. Neugebauer, A. Balogh, and W. C. Feldman. Interplanetary discontinuities and Alfvén waves at high heliographic latitudes: Ulysses. *J. Geophys. Res.*, 101(A5):11027–11038, May 1996.
- [7] A. Söding, F. M. Neubauer, B. T. Tsurutani, N. F. Ness, and R. P. Lepping. Radial and latitudinal dependencies of discontinuities in the solar wind between 0.3 and 19 AU and -80 and +10 degrees. *Annales Geophysicae*, 19:681–686, July 2001.
- [8] B. J. Vasquez, V. I. Abramenko, D. K. Haggerty, and C. W. Smith. Numerous small magnetic field discontinuities of Bartels rotation 2286 and the potential role of Alfvénic turbulence. *Journal of Geophysical Research (Space Physics)*, 112:A11102, November 2007.
- [9] S. Perri, M. L. Goldstein, J. C. Dorelli, and F. Sahraoui. Detection of Small-Scale Structures in the Dissipation Regime of Solar-Wind Turbulence. *Phys. Rev. Lett.*, 109(19):191101, November 2012.
- [10] John J. Podesta. The most intense current sheets in the high-speed solar wind near 1 AU. *Journal of Geophysical Research (Space Physics)*, 122(3):2795–2823, March 2017.
- [11] Anton V. Artemyev, Vassilis Angelopoulos, Jasper S. Halekas, Alexander A. Vinogradov, Ivan Y. Vasko, and Lev M. Zelenyi. Dynamics of Intense Currents in the Solar Wind. *Astrophys. J.*, 859(2):95, Jun 2018.
- [12] I. Y. Vasko, K. Alimov, T. D. Phan, S. D. Bale, F. S. Mozer, and A. V. Artemyev. Kinetic-scale Current Sheets in the Solar Wind at 1 au: Properties and the Necessary Condition for Reconnection. *Astrophys. J. Lett.*, 923(1):L19, December 2021.
- [13] I. Y. Vasko, K. Alimov, T. Phan, S. D. Bale, F. S. Mozer, and A. V. Artemyev. Kinetic-scale Current Sheets in the Solar Wind at 1 au: Scale-dependent Properties and Critical Current Density. *Astrophys. J. Lett.*, 926(2):L19, February 2022.
- [14] A. B. Lotekar, I. Y. Vasko, T. Phan, S. D. Bale, T. A. Bowen, J. Halekas, A. V. Artemyev, Yu. V. Khotyaintsev, and F. S. Mozer. Kinetic-scale Current Sheets in Near-Sun Solar Wind: Properties, Scale-dependent Features and Reconnection Onset. *Astrophys. J.*, 929(1):58, April 2022.
- [15] J. E. Borovsky. Contribution of Strong Discontinuities to the Power Spectrum of the Solar Wind. *Physical Review Letters*, 105(11):111102, September 2010.
- [16] John J. Podesta and Joseph E. Borovsky. Relationship between the durations of jumps in solar wind time series and the frequency of the spectral break. *Journal of Geophysical Research (Space Physics)*, 121(3):1817–1838, March 2016.
- [17] Joseph E. Borovsky and Michael H. Denton. No Evidence for Heating of the Solar Wind at Strong Current Sheets. *Astrophys. J. Lett.*, 739(2):L61, October 2011.
- [18] K. T. Osman, W. H. Matthaeus, M. Wan, and A. F. Rappazzo. Intermittency and Local Heating in the Solar Wind. *Phys. Rev. Lett.*, 108(26):261102, June 2012.
- [19] P. Wu, S. Perri, K. Osman, M. Wan, W. H. Matthaeus, M. A. Shay, M. L. Goldstein, H. Karimabadi, and S. Chapman. Intermittent Heating in Solar Wind and Kinetic Simulations. *Astrophys. J. Lett.*, 763(2):L30, February 2013.
- [20] Nikos Sioulas, Marco Velli, Rohit Chhiber, Loukas Vlahos, William H. Matthaeus, Riddhi Bandyopadhyay, Manuel E. Cuesta, Chen Shi, Trevor A. Bowen, Ramiz A. Qudsi, Michael L. Stevens, and Stuart D. Bale. Statistical Analysis of Intermittency and its Association with Proton Heating in the Near-Sun Environment. *Astrophys. J.*, 927(2):140, March 2022.
- [21] R. Bruno, V. Carbone, P. Veltri, E. Pietropaolo, and B. Bavassano. Identifying intermittency events in the solar wind. *Plan. Sp. Sci.*, 49(12):1201–1210, October 2001.
- [22] Joseph E. Borovsky. Flux tube texture of the solar wind: Strands of the magnetic carpet at 1 AU? *Journal of Geophysical Research (Space Physics)*, 113(A8):A08110, August 2008.
- [23] A. Greco, P. Chuychai, W. H. Matthaeus, S. Servidio, and P. Dmitruk. Intermittent MHD structures and classical discontinuities. *Geophys. Res. Lett.*, 35:L19111, October 2008.
- [24] A. Greco, W. H. Matthaeus, S. Servidio, P. Chuychai, and P. Dmitruk. Statistical Analysis of Discontinuities in Solar Wind ACE Data and Comparison with Intermittent MHD Turbulence. *Astrophys. J. Lett.*, 691(2):L111–L114, February 2009.
- [25] Vladimir Zhdankin, Stanislav Boldyrev, and Joanne Mason. Distribution of Magnetic Discontinuities in the Solar Wind and in Magnetohydrodynamic Turbulence. *Astrophys. J. Lett.*, 760(2):L22, December 2012.

- [26] H. Karimabadi, V. Roytershteyn, M. Wan, W. H. Matthaeus, W. Daughton, P. Wu, M. Shay, B. Loring, J. Borovsky, E. Leonardis, S. C. Chapman, and T. K. M. Nakamura. Coherent structures, intermittent turbulence, and dissipation in high-temperature plasmas. *Physics of Plasmas*, 20(1):012303, January 2013.
- [27] Vladimir Zhdankin, Dmitri A. Uzdensky, Jean C. Perez, and Stanislav Boldyrev. Statistical Analysis of Current Sheets in Three-dimensional Magnetohydrodynamic Turbulence. *Astrophys. J.*, 771(2):124, July 2013.
- [28] Vladimir Zhdankin, Stanislav Boldyrev, Jean Carlos Perez, and Steven M. Tobias. Energy Dissipation in Magnetohydrodynamic Turbulence: Coherent Structures or “Nanoflares”? *Astrophys. J.*, 795(2):127, November 2014.
- [29] M. Wan, W. H. Matthaeus, H. Karimabadi, V. Roytershteyn, M. Shay, P. Wu, W. Daughton, B. Loring, and S. C. Chapman. Intermittent Dissipation at Kinetic Scales in Collisionless Plasma Turbulence. *Phys. Rev. Lett.*, 109(19):195001, November 2012.
- [30] M. Wan, W. H. Matthaeus, V. Roytershteyn, T. N. Parashar, P. Wu, and H. Karimabadi. Intermittency, coherent structures and dissipation in plasma turbulence. *Physics of Plasmas*, 23(4):042307, April 2016.
- [31] M. Sisti, S. Fadanelli, S. S. Cerri, M. Faganello, F. Califano, and O. Agullo. Characterizing current structures in 3D hybrid-kinetic simulations of plasma turbulence. *Astronomy and Astrophysics*, 655:A107, November 2021.
- [32] Neeraj Jain, Jörg Büchner, Horia Comişel, and Uwe Motschmann. Free Energy Sources in Current Sheets Formed in Collisionless Plasma Turbulence. *Astrophys. J.*, 919(2):103, October 2021.
- [33] J. T. Gosling, T. D. Phan, R. P. Lin, and A. Szabo. Prevalence of magnetic reconnection at small field shear angles in the solar wind. *Geophys. Res. Lett.*, 34(15):L15110, August 2007.
- [34] J. T. Gosling and A. Szabo. Bifurcated current sheets produced by magnetic reconnection in the solar wind. *Journal of Geophysical Research (Space Physics)*, 113(A10):A10103, October 2008.
- [35] R. Mistry, J. P. Eastwood, T. D. Phan, and H. Hietala. Statistical properties of solar wind reconnection exhausts. *Journal of Geophysical Research (Space Physics)*, 122(6):5895–5909, June 2017.
- [36] T. D. Phan, J. T. Gosling, M. S. Davis, R. M. Skoug, M. Øieroset, R. P. Lin, R. P. Lepping, D. J. McComas, C. W. Smith, H. Reme, and A. Balogh. A magnetic reconnection X-line extending more than 390 Earth radii in the solar wind. *Nature*, 439(7073):175–178, January 2006.
- [37] T. D. Phan, J. T. Gosling, and M. S. Davis. Prevalence of extended reconnection X-lines in the solar wind at 1 AU. *Geophys. Res. Lett.*, 36(9):L09108, May 2009.
- [38] T. D. Phan, J. T. Gosling, G. Paschmann, C. Pasma, J. F. Drake, M. Øieroset, D. Larson, R. P. Lin, and M. S. Davis. The Dependence of Magnetic Reconnection on Plasma  $\beta$  and Magnetic Shear: Evidence from Solar Wind Observations. *Astrophys. J. Lett.*, 719:L199–L203, August 2010.
- [39] T. D. Phan, S. D. Bale, J. P. Eastwood, B. Lavraud, J. F. Drake, M. Oieroset, M. A. Shay, M. Pulupa, M. Stevens, R. J. MacDowall, A. W. Case, D. Larson, J. Kasper, P. Whittlesey, A. Szabo, K. E. Korreck, J. W. Bonnell, T. Dudok de Wit, K. Goetz, P. R. Harvey, T. S. Horbury, R. Livi, D. Malaspina, K. Paulson, N. E. Raouafi, and M. Velli. Parker Solar Probe In Situ Observations of Magnetic Reconnection Exhausts during Encounter 1. *Astrophys. Journal. Suppl. Ser.*, 246(2):34, February 2020.
- [40] Stefan Eriksson, Marc Swisdak, James M. Weygand, Alfred Mallet, David L. Newman, Giovanni Lapenta, III Wilson, Lynn B., Drew L. Turner, and Bjorn Larsen. Characteristics of Multi-scale Current Sheets in the Solar Wind at 1 au Associated with Magnetic Reconnection and the Case for a Heliospheric Current Sheet Avalanche. *Astrophys. J.*, 933(2):181, July 2022.
- [41] S. Servidio, W. H. Matthaeus, M. A. Shay, P. A. Cassak, and P. Dmitruk. Magnetic Reconnection in Two-Dimensional Magnetohydrodynamic Turbulence. *Phys. Rev. Lett.*, 102(11):115003, March 2009.
- [42] S. Servidio, A. Greco, W. H. Matthaeus, K. T. Osman, and P. Dmitruk. Statistical association of discontinuities and reconnection in magnetohydrodynamic turbulence. *Journal of Geophysical Research (Space Physics)*, 116:A09102, September 2011.
- [43] S. S. Cerri and F. Califano. Reconnection and small-scale fields in 2D-3V hybrid-kinetic driven turbulence simulations. *New Journal of Physics*, 19(2):025007, February 2017.
- [44] Luca Franci, Silvio Sergio Cerri, Francesco Califano, Simone Landi, Emanuele Papini, Andrea Verdini, Lorenzo Matteini, Frank Jenko, and Petr Hellinger. Magnetic Reconnection as a Driver for a Sub-ion-scale Cascade in Plasma Turbulence. *Astrophys. J. Lett.*, 850(1):L16, November 2017.
- [45] Emanuele Papini, Luca Franci, Simone Landi, Andrea Verdini, Lorenzo Matteini, and Petr Hellinger. Can Hall Magnetohydrodynamics Explain Plasma Turbulence at Sub-ion Scales? *Astrophys. J.*, 870(1):52, January 2019.

- [46] M. Neugebauer, D. R. Clay, B. E. Goldstein, B. T. Tsurutani, and R. D. Zwickl. A reexamination of rotational and tangential discontinuities in the solar wind. *J. Geophys. Res.*, 89(A7):5395–5408, July 1984.
- [47] Timothy S. Horbury, David Burgess, Markus Fränz, and Christopher J. Owen. Three spacecraft observations of solar wind discontinuities. *Geophys. Res. Lett.*, 28(4):677–680, January 2001.
- [48] T. Knetter, F. M. Neubauer, T. Horbury, and A. Balogh. Four-point discontinuity observations using Cluster magnetic field data: A statistical survey. *Journal of Geophysical Research (Space Physics)*, 109:A06102, June 2004.
- [49] M. Neugebauer. Comment on the abundances of rotational and tangential discontinuities in the solar wind. *Journal of Geophysical Research (Space Physics)*, 111:A04103, April 2006.
- [50] G. Paschmann, S. Haaland, B. Sonnerup, and T. Knetter. Discontinuities and Alfvénic fluctuations in the solar wind. *Annales Geophysicae*, 31(5):871–887, May 2013.
- [51] A. V. Artemyev, V. Angelopoulos, and I. Y. Vasko. Kinetic Properties of Solar Wind Discontinuities at 1 AU Observed by ARTEMIS. *Journal of Geophysical Research (Space Physics)*, 124(6):3858–3870, June 2019.
- [52] A. V. Artemyev, V. Angelopoulos, and I. Y. Vasko. Kinetic Properties of Solar Wind Discontinuities at 1 AU Observed by ARTEMIS. *Journal of Geophysical Research (Space Physics)*, 124(6):3858–3870, June 2019.
- [53] J. T. Gosling and T. D. Phan. Magnetic Reconnection in the Solar Wind at Current Sheets Associated with Extremely Small Field Shear Angles. *Astrophys. J. Lett.*, 763(2):L39, February 2013.
- [54] C. P. Escoubet, M. Fehringer, and M. Goldstein. Introduction: The Cluster mission. *Annales Geophysicae*, 19:1197–1200, October 2001.
- [55] C. P. Escoubet, A. Masson, H. Laakso, M. L. Goldstein, T. Dimbylow, Y. V. Bogdanova, M. Hapgood, B. Sousa, D. Sieg, and M. G. G. T. Taylor. Cluster After 20 Years of Operations: Science Highlights and Technical Challenges. *Journal of Geophysical Research (Space Physics)*, 126(8):e29474, August 2021.
- [56] A. Balogh, C. M. Carr, M. H. Acuña, M. W. Dunlop, T. J. Beek, P. Brown, K. H. Fornaçon, E. Georgescu, K. H. Glassmeier, J. Harris, G. Musmann, T. Oddy, and K. Schwingenschuh. The Cluster Magnetic Field Investigation: overview of in-flight performance and initial results. *Annales Geophysicae*, 19(10):1207–1217, October 2001.
- [57] H. Rème, C. Aoustin, J. M. Bosqued, I. Dandouras, B. Lavraud, J. A. Sauvaud, A. Barthe, J. Bouyssou, Th. Camus, O. Coeur-Joly, A. Cros, J. Cuvalo, F. Ducay, Y. Garbarowitz, J. L. Medale, E. Penou, H. Perrier, D. Romefort, J. Rouzaud, C. Vallat, D. Alcaydé, C. Jacquy, C. Mazelle, C. D’Uston, E. Möbius, L. M. Kistler, K. Crocker, M. Granoff, C. Mouikis, M. Popecki, M. Vosbury, B. Klecker, D. Hovestadt, H. Kucharek, E. Kueneth, G. Paschmann, M. Scholer, N. Scopke (), E. Seidenschwang, C. W. Carlson, D. W. Curtis, C. Ingraham, R. P. Lin, J. P. McFadden, G. K. Parks, T. Phan, V. Formisano, E. Amata, M. B. Bavassano-Cattaneo, P. Baldetti, R. Bruno, G. Chionchio, A. di Lellis, M. F. Marcucci, G. Palocchia, A. Korth, P. W. Daly, B. Graeve, H. Rosenbauer, V. Vasyliunas, M. McCarthy, M. Wilber, L. Eliasson, R. Lundin, S. Olsen, E. G. Shelley, S. Fuselier, A. G. Ghielmetti, W. Lennartsson, C. P. Escoubet, H. Balsiger, R. Friedel, J. B. Cao, R. A. Kovrazhkin, I. Papamastorakis, R. Pellat, J. Scudder, and B. Sonnerup. First multispacecraft ion measurements in and near the Earth’s magnetosphere with the identical Cluster ion spectrometry (CIS) experiment. *Annales Geophysicae*, 19:1303–1354, October 2001.
- [58] P. M. E. Décréau, P. Ferreau, V. Krasnoselskikh, E. Le Guirriec, M. Lévêque, Ph. Martin, O. Randriamboarison, J. L. Rauch, F. X. Sené, H. C. Séran, J. G. Trotignon, P. Canu, N. Cornilleau, H. de Féraudy, H. Alleyne, K. Yearby, P. B. Mögensen, G. Gustafsson, M. André, D. C. Gurnett, F. Darrouzet, J. Lemaire, C. C. Harvey, P. Travnicek, and Whisper Experimenters Group. Early results from the Whisper instrument on Cluster: an overview. *Annales Geophysicae*, 19(10):1241–1258, October 2001.
- [59] A. D. Johnstone, C. Alsop, S. Burge, P. J. Carter, A. J. Coates, A. J. Coker, A. N. Fazakerley, M. Grande, R. A. Gowen, C. Gurgiolo, B. K. Hancock, B. Narheim, A. Preece, P. H. Sheather, J. D. Winningham, and R. D. Woodliffe. Peace: a Plasma Electron and Current Experiment. *Space Sci. Rev.*, 79:351–398, January 1997.
- [60] III Wilson, Lynn B., Alexandra L. Brosius, Natchimuthuk Gopalswamy, Teresa Nieves-Chinchilla, Adam Szabo, Kevin Hurley, Tai Phan, Justin C. Kasper, Noé Lugaz, Ian G. Richardson, Christopher H. K. Chen, Daniel Verscharen, Robert T. Wicks, and Jason M. TenBerge. A Quarter Century of Wind Spacecraft Discoveries. *Reviews of Geophysics*, 59(2):e2020RG000714, May 2021.
- [61] A. Greco, W. H. Matthaeus, S. Perri, K. T. Osman, S. Servidio, M. Wan, and P. Dmitruk. Partial Variance of Increments Method in Solar Wind Observations and Plasma Simulations. *Space Sci. Rev.*, 214(1):1, Feb 2018.
- [62] W. H. Matthaeus, S. Dasso, J. M. Weygand, L. J. Milano, C. W. Smith, and M. G. Kivelson. Spatial Correlation of Solar-Wind Turbulence from Two-Point Measurements. *Phys. Rev. Lett.*, 95(23):231101, December 2005.
- [63] B. U. Ö. Sonnerup and M. Scheible. Minimum and Maximum Variance Analysis. *ISSI Scientific Reports Series*, 1:185–220, 1998.

- [64] Roberto Bruno. Intermittency in Solar Wind Turbulence From Fluid to Kinetic Scales. *Earth and Space Science*, 6(5):656–672, May 2019.
- [65] A. Greco, S. Perri, S. Servidio, E. Yordanova, and P. Veltri. The Complex Structure of Magnetic Field Discontinuities in the Turbulent Solar Wind. *Astrophys. J. Lett.*, 823(2):L39, June 2016.
- [66] R. Wang, I. Y. Vasko, A. V. Artemyev, L. C. Holley, S. R. Kamaletdinov, A. Lotekar, and F. S. Mozer. Multisatellite Observations of Ion Holes in the Earth’s Plasma Sheet. *Geophys. Res. Lett.*, 49(8):e97919, April 2022.
- [67] I. Y. Vasko, A. V. Artemyev, A. A. Petrukovich, R. Nakamura, and L. M. Zelenyi. The structure of strongly tilted current sheets in the Earth magnetotail. *Annales Geophysicae*, 32(2):133–146, Feb 2014.
- [68] R. P. Lepping and K. W. Behannon. Magnetic field directional discontinuities: 1. Minimum variance errors. *J. Geophys. Res.*, 85(A9):4695–4704, September 1980.
- [69] Y. Y. Liu, H. S. Fu, J. B. Cao, Y. Yu, C. M. Liu, Z. Wang, Z. Z. Guo, and R. J. He. Categorizing MHD Discontinuities in the Inner Heliosphere by Utilizing the PSP Mission. *Journal of Geophysical Research (Space Physics)*, 127(3):e29983, March 2022.
- [70] Charles W. Smith, Bernard J. Vasquez, and Kathleen Hamilton. Interplanetary magnetic fluctuation anisotropy in the inertial range. *Journal of Geophysical Research (Space Physics)*, 111(A9):A09111, September 2006.
- [71] Kathleen Hamilton, Charles W. Smith, Bernard J. Vasquez, and Robert J. Leamon. Anisotropies and helicities in the solar wind inertial and dissipation ranges at 1 AU. *Journal of Geophysical Research (Space Physics)*, 113(A1):A01106, January 2008.
- [72] C. H. K. Chen. Recent progress in astrophysical plasma turbulence from solar wind observations. *Journal of Plasma Physics*, 82(6):535820602, December 2016.
- [73] V. Krasnoselskikh, A. Larosa, O. Agapitov, T. Dudok de Wit, M. Moncuquet, F. S. Mozer, M. Stevens, S. D. Bale, J. Bonnell, C. Froment, K. Goetz, K. Goodrich, P. Harvey, J. Kasper, R. MacDowall, D. Malaspina, M. Pulupa, N. Raouafi, C. Revillet, M. Velli, and J. Wygant. Localized Magnetic-field Structures and Their Boundaries in the Near-Sun Solar Wind from Parker Solar Probe Measurements. *Astrophys. J.*, 893(2):93, April 2020.
- [74] A. Larosa, V. Krasnoselskikh, T. Dudok de Wit, O. Agapitov, C. Froment, V. K. Jagarlamudi, M. Velli, S. D. Bale, A. W. Case, K. Goetz, P. Harvey, J. C. Kasper, K. E. Korreck, D. E. Larson, R. J. MacDowall, D. Malaspina, M. Pulupa, C. Revillet, and M. L. Stevens. Switchbacks: statistical properties and deviations from Alfvénicity. *Astronomy and Astrophysics*, 650:A3, June 2021.
- [75] M. Akhavan-Tafti, J. Kasper, J. Huang, and S. Bale. Discontinuity analysis of the leading switchback transition regions. *Astronomy and Astrophysics*, 650:A4, June 2021.
- [76] Alexandros Chasapis, W. H. Matthaeus, T. N. Parashar, S. A. Fuselier, B. A. Maruca, T. D. Phan, J. L. Burch, T. E. Moore, C. J. Pollock, D. J. Gershman, R. B. Torbert, C. T. Russell, and R. J. Strangeway. High-resolution Statistics of Solar Wind Turbulence at Kinetic Scales Using the Magnetospheric Multiscale Mission. *Astrophys. J. Lett.*, 844(1):L9, July 2017.
- [77] E. Papini, S. Landi, and L. Del Zanna. Fast Magnetic Reconnection: Secondary Tearing Instability and Role of the Hall Term. *Astrophys. J.*, 885(1):56, November 2019.
- [78] Amirhassan Chatraee Azizabadi, Neeraj Jain, and Jörg Büchner. Identification and characterization of current sheets in collisionless plasma turbulence. *Physics of Plasmas*, 28(5):052904, May 2021.
- [79] J. V. Shebalin, W. H. Matthaeus, and D. Montgomery. Anisotropy in MHD turbulence due to a mean magnetic field. *Journal of Plasma Physics*, 29(3):525–547, June 1983.
- [80] Stanislav Boldyrev. Spectrum of Magnetohydrodynamic Turbulence. *Phys. Rev. Lett.*, 96(11):115002, March 2006.
- [81] Nuno F. Loureiro and Stanislav Boldyrev. Collisionless Reconnection in Magnetohydrodynamic and Kinetic Turbulence. *Astrophys. J.*, 850(2):182, December 2017.
- [82] A. Mallet, A. A. Schekochihin, and B. D. G. Chandran. Disruption of sheet-like structures in Alfvénic turbulence by magnetic reconnection. *Mon. Not. Royal. Soc.*, 468(4):4862–4871, July 2017.